Three-dimensional hybrid solitary waves: Transverse vortex solitons stabilized by longitudinal parametric solitary waves

Antonio Picozzi

Laboratoire de Physique de la Matière Condensée, CNRS-UMR 6622, Université de Nice Sophia-Antipolis, Parc Valrose, F-06108 Nice Cedex, France

We show that the parametric process in quadratic nonlinear media supports three-dimensional (3D) hybrid solitary wave solution in which a transverse vortex solitons embedded in an infinite plane-wave background is sustained by a longitudinal parametric solitary wave. The structure of the parametric solitary wave results from the interplay of the quadratic nonlinearity and the temporal walk off (i.e., the velocity mismatch) between the interacting waves. The 3D hybrid solitary wave proved to be robust with respect to modulational instability, a feature that contrasts with previous studies on quadratic vortex solitons that revealed them to be always modulationally unstable. We show that the mechanism of stabilization of the vortex background lies on the temporal walkoff between the interacting waves that is able to drift the modulational instability out of the temporally localized structure that constitutes the 3D hybrid solitary wave.

I. INTRODUCTION

Vortices or screw phase dislocations are ubiquitous entities encountered in many branches of physics [1]. They constitute topological phase singularities of a complex field in which the field intensity vanishes at the singular point while the phase changes by $2\pi m$ (m being an integer, the vortex charge) along any closed loop around the zero intensity point. Vortices have been widely investigated in optics in several settings such as, e.g., in optical cavities or speckle fields. When an optical vortex is generated in a linear bulk medium, it expands during the propagation due to the effect of diffraction. However the expansion of the vortex core can be compensated in a nonlinear defocusing medium owing to the nonlinearity-induced change of the refractive index, thereby creating a stationary structure, i.e., *an optical vortex soliton* [2,3].

Optical vortex solitons have been extensively investigated from both the theoretical and experimental viewpoints in cubic nonlinear media where they are known as stable two-dimensional structures [2,3]. In these last few years, a considerable effort has been realized to generalize the optical vortex solitons to *quadratic nonlinear media*. The quadratic interaction is interesting since it provides an efficient way of vortex transformation by mixing waves of different frequencies, which has been recently investigated experimentally [4]. However, straightforward extension of the concept of vortex soliton to the case of quadratic nonlinearities fails. Indeed, it has been shown theoretically that all finite-amplitude plane waves suffer from parametric modulational instability [5]. As a result, no stable vortex solitons have been found to exist in a pure quadratic medium. Most recently, it has been shown that a weak defocusing cubic nonlinearity can eliminate the parametric modulational instability of plane waves, leading to a stabilization of the vortex soliton [6,7]. Another mechanism of stabilization has been recently proposed: In the situation where the background of the vortex soliton ''is not too large'' [8], a *transverse spatial*

walkoff can drift the modulational instability of the vortex background out of the beam itself. This mechanism of self-quenching of the parametric modulational instability allowed for the observation of the quadratic vortex soliton when it is embedded in a *finite* beam background [8].

In the present paper, we address the problem of the generation of stable quadratic vortex solitons embedded in an infinite plane-wave background from a different point of view. The original idea, recently suggested in Ref. [8] that the transverse spatial walk off is able to stabilize the two-dimensional (2D) vortex soliton embedded in a *finite* background, may be extended to 3D in order to stabilize vortex solitons embedded in an *infinite* background. This may be achieved by considering a *temporal* walkoff along the longitudinal axis of propagation instead of a *spatial* walkoff in the transverse plane of the optical beam, as suggested in Ref. [8]. Indeed, it is well known that a strong temporal walkoff is responsible for the spontaneous localization of the optical fields along the longitudinal axis of propagation. This longitudinal localization allows for the modulational instability to drift out of the temporally localized structure before it has time to develop. Since the drift of the modulational instability takes place along the longitudinal axis of propagation, this mechanism of self-stabilization occurs for any transverse profile of the field envelopes, in particular, for the transverse vortex profile embedded in an infinite plane-wave background.

Beside this self-stabilization mechanism, we show that, quite remarkably, the longitudinal localization of the interacting fields results in the formation of a *parametric solitary wave* [9]. This type of solitary wave results from an exact balance between the parametric nonlinear process and the velocity mismatch between the interacting waves, i.e., the temporal walk off. The parametric solitary waves have been extensively investigated in the pure 1D case in various contexts of nonlinear optics [10,11], in particular, in quadratic nonlinear media [12–14]. In the multidimensional case of interest here, the longitudinal parametric solitary wave is coupled to the transverse vortex soliton to form a 3D *hybrid*

solitary wave. In this way, the proposed 3D solitary wave generalizes the previously reported 2D hybrid solitary wave [15] by including in the solitary wave structure the transverse vortex soliton owing to an additional transverse dimension. The main issue lies on the robustness of the 3D hybrid solitary wave with respect to the modulational instability of the transverse vortex background. We show that this robustness results from the self-stabilization mechanism that originates in the temporal walkoff between the fields that constitute the 3D hybrid solitary wave.

Both the 3D hybrid solitary wave solution and the associated process of self-stabilization of the plane-wave vortex background constitute the subject of the present article. The 3D solitary wave proposed here is also relevant to the recently reported composite vector solitons carrying a topological charge [16] or to spatiotemporal solitons that are of particular interest in quadratic nonlinear media where recent experiments have been performed [17].

II. GOVERNING EQUATIONS

We consider the usual three-wave interaction model that govern the spatiotemporal evolution of optical fields in a nonlinear quadratic crystal. The evolution of the slowly varying envelopes u_i of these fields of frequency ω_i and wave number k_i obey the coupled partial differential equations

$$\frac{\partial u_1}{\partial t'} + v_1 \frac{\partial u_1}{\partial z'} + \gamma_1 u_1 = \sigma_1 u_3 u_2^* + i\rho_1 \nabla_\perp^2 u_1, \qquad (1a)$$

$$\frac{\partial u_2}{\partial t'} + v_2 \frac{\partial u_2}{\partial z'} + \gamma_2 u_2 = \sigma_2 u_3 u_1^* + i\rho_2 \nabla_\perp^2 u_2, \qquad (1b)$$

$$\frac{\partial u_3}{\partial t'} + v_3 \frac{\partial u_3}{\partial z'} + \gamma_3 u_3 = -\sigma_3 u_2 u_1 + i\rho_3 \nabla_\perp^2 u_3, \qquad (1c)$$

where $\nabla_\perp^2 = \partial^2/\partial x'^2 + \partial^2/\partial y'^2$, x' and y' being the transverse spatial coordinates. For definiteness we call u_1, u_2, u_3 the signal, idler, and pump waves, respectively. v_i are the group velocities of the three waves along the longitudinal z' axis and γ_i are their attenuation coefficients. The nonlinear coefficients are $\sigma_i = 2\pi d v_i/\lambda_i n_i$ where n_i is the refractive index at frequency ω_i and d is the effective nonlinear susceptibility. The effect of diffraction is taken into account in Eqs. (1) through the parameters $\eta_i = \rho_i v_i$, where $\rho_i = 1/2k_i$ are the diffraction coefficients.

Since our aim here is to study the influence of the temporal walk off on the transverse dynamics of the vortex structure, we will consider for the sake of simplicity that there is a walk off only between the signal and the pump-idler fields, i.e., we assume that the pump and idler waves propagate with the same group velocity $v_2 = v_3$. This assumption allows us to define a unique parameter $\delta = (v_{2,3} - v_1)/2$ that represents the amount of walk off between the interacting waves.

Owing to this assumption, we now write Eqs. (1) in the reference frame traveling at the average group velocity $(v_1 + v_{2,3})/2$ of the signal and the comoving pump and idler waves, we thus define the new variable $z'' = z' - \delta t'$. The
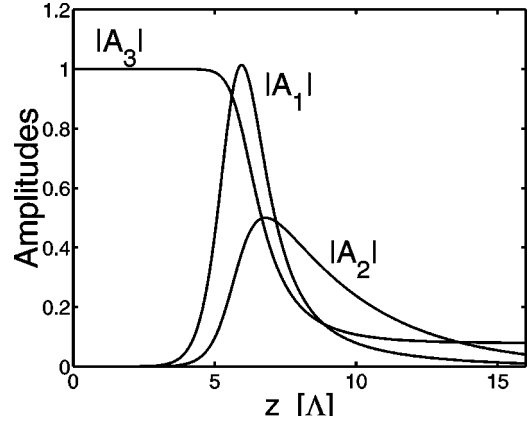

FIG. 1. Typical envelopes profiles of the parametric solitary wave solution in the pure one-dimensional case. Parameters are $\kappa = 0$, $\mu_1 = 0.3$, $\mu_2 = 0.6$, $\mu_3 = 0$ (amplitudes are given in units of e_0).

choice of this particular reference frame may appear artificial at this point, however, the reason for this choice will become clear later. Note that, without loss of generality, we will assume in the following that $v_1 < v_{2,3}$. For convenience, we also write Eqs. (1) in a normalized form: the field amplitudes u_i, the time t', the damping rates γ_i and the spatial coordinates (x', y', z'') are normalized with respect to the pump amplitude e_0 at the input of the crystal and with respect to the characteristic evolution time of the parametric interaction $\tau_0 = (\sigma_1 e_0)^{-1}$. The corresponding characteristic interaction length then reads $\Lambda = \delta\tau_0$. In dimensionless units, Eqs. (1) then take the following form

$$\frac{\partial A_1}{\partial t} - \frac{\partial A_1}{\partial z} + \mu_1 A_1 = A_3 A_2^* + i\kappa_1 \nabla_\perp^2 A_1, \qquad (2a)$$

$$\frac{\partial A_2}{\partial t} + \frac{\partial A_2}{\partial z} + \mu_2 A_2 = r_2 A_3 A_1^* + i\kappa_2 \nabla_\perp^2 A_2, \qquad (2b)$$

$$\frac{\partial A_3}{\partial t} + \frac{\partial A_3}{\partial z} + \mu_3 A_3 = -r_3 A_2 A_1 + i\kappa_3 \nabla_\perp^2 A_3, \qquad (2c)$$

where the variables in real units are related to the dimensionless variables through the transformation $u_i = A_i e_0$, $t' = t\tau_0$, $(x', y', z'') = (x, y, z)\delta\tau_0$, $\gamma_i = \mu_i/\tau_0$. In these units, the normalized diffraction coefficients in Eqs. (2) are $\kappa_i = v_i \rho_i/\delta^2 \tau_0$, while the normalized nonlinear susceptibility is $r_i = \sigma_i/\sigma_1$ $(i = 2,3)$. In the following, we will assume for simplicity that $r_3 = 2r_2 = 2$ and $\kappa = \kappa_1 = \kappa_2 = 2\kappa_3$. As will be discussed in Sec. V, these assumptions are consistent with realistic experimental configurations.

III. SYMMETRY CONSIDERATIONS

In a recent work we investigated Eqs. (2) in the pure one-dimensional case $(\kappa_i = 0)$ and found a family of parametric solitary wave solutions [13] whose typical envelopes profiles A_i are illustrated in Fig. 1. The longitudinal confinement of the down-converted signal and idler fields results from the interplay of the parametric amplification from the
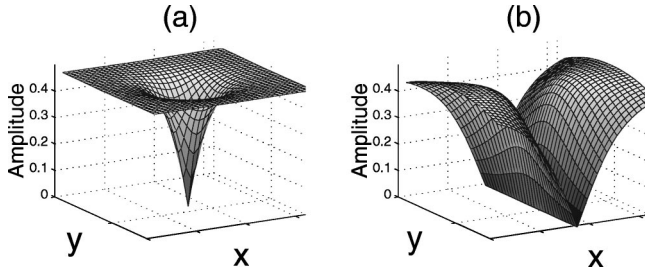
FIG. 2. Typical evolution, after few interactions times ($t=4$), of the parametric amplification from a plane-wave pump of an initial vortex profile: the nondegenerate configuration of the parametric process preserves the vortex structure (a), whereas in the degenerate configuration, the initial vortex evolves to a stripe pattern (b).

continuous pump and the velocity mismatch between the interacting waves (i.e., the temporal walkoff). We investigate here a 3D hybrid structure in which the longitudinal parametric solitary wave sustains a transverse vortex soliton in the transverse plane (x,y) [$\kappa_i \neq 0$ in Eqs. (2)]. In this respect, let us make some preliminary remarks on the simpler problem of the parametric amplification of a vortex structure from a plane-wave pump.

An important aspect to point out is that the plane-wave pump can only sustain a vortex structure when the parametric process takes place in the *nondegenerate configuration*. This may be easily seen by invoking some simple symmetries considerations. Indeed, one can easily verify that Eqs. (2) are invariant under the transformation $(A_1, A_2, A_3) \rightarrow (A_1 \exp[i\phi], A_2 \exp[-i\phi], A_3)$, where ϕ is an arbitrary constant phase. Owing to this particular symmetry associated with the continuous variable ϕ, we may anticipate that the vortex structure of the down-converted fields $A_{1,2}$ is preserved when the amplification process is driven by a plane-wave pump $A_3 = cte$ [1]. Conversely, when the parametric process takes place in the *degenerate* configuration ($\omega_1 = \omega_2, A_1 = A_2$), the previous continuous symmetry reduces to the following discrete symmetry $(A_1, A_3) \rightarrow (-A_1, A_3)$ and we may expect that the vortex structure of the signal beam A_1 is no longer preserved during the amplification process [1].

We checked these predictions by the numerical simulation of Eqs. (2) where we neglected for simplicity the temporal walkoff between the interacting waves. Starting from an initial vortex profile [$A_1(r, \theta, t=0) = \epsilon \tanh(\Delta r)\exp(i\theta)$, (r, θ) being the polar coordinates of the (x,y) plane, ϵ and Δ being constants], we see in Fig. 2(a) that the nondegenerate parametric interaction preserves the vortex structure during the parametric amplification. Conversely, in the degenerate configuration, the initial vortex structure rapidly evolves to a stripe pattern [Fig. 2(b)] that is subsequently preserved during the amplification owing to the specific symmetry of the degenerate parametric process. Note that the vortex-to-stripe evolution is a simple consequence of the phase sensitive nature of the degenerate interaction that results in the amplification of the real part of the signal amplitude A_1 to the detriment of its imaginary part (when the initial pump amplitude $A_3 = cte$ is assumed to be real). Then, as a result the particular symmetry of the degenerate parametric interaction prevents the vortex structure to be conserved during the parametric amplification.

IV. 3D SOLITARY WAVE GENERATION

These simple considerations on the symmetries of the parametric process indicate that the nondegenerate configuration is essential in order to investigate a 3D hybrid solitary wave in which a transverse vortex soliton is sustained by the longitudinal parametric solitary wave. Indeed, owing to the particular symmetry of the nondegenerate configuration, we may anticipate that the parametric growth of the vortex profile would be preserved during the amplification and would form a vortex soliton if it could be stabilized through a mutual compensation of diffraction and nonlinearity. Morever, we may expect that the temporal walkoff, which is inherent to the longitudinal parametric solitary wave, would permit the modulational instability of the vortex background to drift out of the temporally localized structure before it has time to develop. In this regard, the longitudinal parametric solitary wave would play an essential role in the mechanism of stabilization of the plane-wave vortex background. This important aspect as regards the vortex stability will be discussed in details in the next section (Sec. V). Before considering the stability problem, let us discuss first the existence of the 3D hybrid solitary wave.

To investigate numerically the existence and spontaneous formation of the 3D hybrid solitary wave, we consider the parametric amplification of a signal field that exhibits a vortex structure in its transverse profile in the (x,y) plane and that is localized along the longitudinal z axis. Since we are looking for a solitary wave that results from the energy transfer from the pump to the down-converted fields, we have to neglect the loss of the pump wave. Setting $\mu_3 = 0$ is indeed the only way to keep constant the energy transfer from the pump to the signal so as to generate a stationnary field structure. This is a usual approximation for parametric solitary waves [11–15]. Note however that in the presence of pump loss ($\mu_3 \neq 0$), the parametric solitary wave still exists and simply undergoes adiabatic reshaping during propagation to adapt its profile to the local value of the exponentially decreasing pump amplitude.

With this asumption, we solved Eqs. (2) numerically by extending to three dimensions the numerical scheme outlined in Ref. [18]. We considered a cubic grid of $64 \times 64 \times 64$ points, with a window size of $L=16(x=[-8,8], y=[-8,8], z=[0,16])$. In this example the damping parameters are $\mu_1 = 0.3$, $\mu_2 = 0.6$ and the diffraction parameter is $\kappa = 6 \times 10^{-2}$. As the initial condition in $t=0$, we took a plane wave for the pump $A_3(x,y,z,t=0) = 1$ and a zero field for the idler wave $A_2(x,y,z,t=0) = 0$. For the signal, we considered a transverse vortex profile with topological charge $m=1$ that is bounded along the longitudinal axis z: $A_1(r, \theta, z, t=0) = \epsilon \tanh(\Delta r)\exp(i\theta)z(L-z)$ where $\epsilon = 0.05$ and $\Delta = 0.3$. We solved Eqs. (2) numerically to get the evolution of the fields $A_i(x,y,z,t)$ at any time t in the reference frame of the signal wave defined by the variables ($\xi = z + t, \tau = t$). A typical example is shown in Figs. 3 and 4 that illustrate the time evolution of the signal and pump intensi-
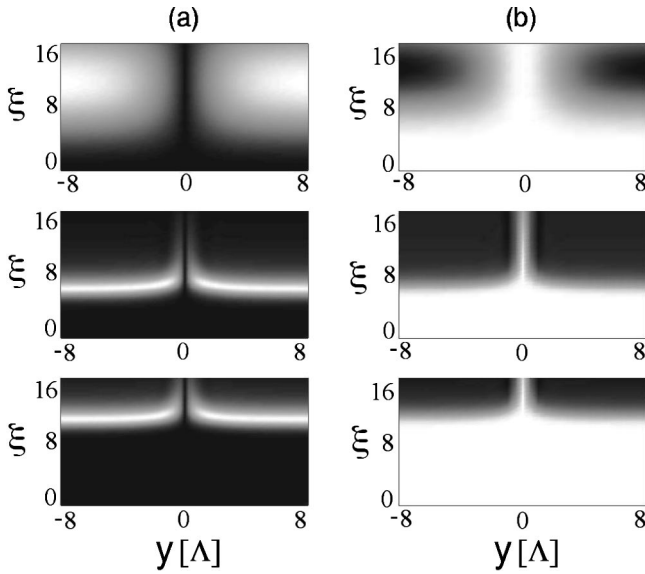
FIG. 3. 3D hybrid solitary wave generation: Evolution of the signal (a) and pump (b) amplitudes $|A_{1,3}|$ (in the signal reference frame, $\xi=z+t$, $\tau=t$) along the longitudinal (z) and transverse (y) axes in the plane $x=0$. After a transient ($t>40$), the optical fields self-structurate in the form of a steady structure that propagates uniformly along the longitudinal z axis. Parameters are $\kappa=6 \times 10^{-2}$, $\mu_1=0.3$, $\mu_2=0.6$ and the window size is $L=16\Lambda$.

ties $|A_{1,3}|$. Figure 3 represents the evolution of the amplitudes $|A_{1,3}|$ in the plane $x=0$, which includes the line of the vortex core where the signal field vanishes $A_1(x=0,y=0,z,t=0)=0$. Figure 4 represents the amplitudes $|A_{1,3}|$ in the proximity of the vortex core in the plane $x=1$. Note that the same results are obtained by plotting the signal and pump intensities in the planes $y=0$ and $y=1$, respectively, which confirms that the generated three-dimensional structure presents a circular symmetry in the transverse plane (x,y).

After a complex transient ($t>40$), the three interacting waves self-organize in the form of the anticipated 3D hybrid solitary wave that is characterized by a parametric solitary wave along the longitudinal z axis and a vortex soliton in the transverse (x,y) plane. Figure 5 shows a typical longitudinal profile of the three interacting fields in the asymptotic regime of the hybrid solitary wave ($t=45$). As evidenced by comparing Figs. 5 and 1, the three envelopes self-structurate
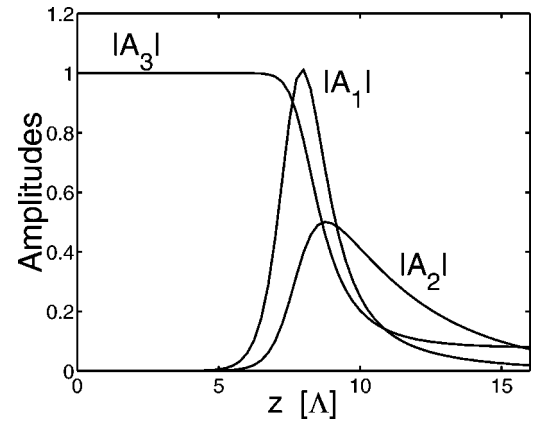
FIG. 5. Typical longitudinal profile of the 3D hybrid solitary wave along the z axis: the amplitudes $|A_i|$ are plotted along the line $(x=5,y=5)$. Parameters are the same as in Fig. 3 (amplitudes are given in units of e_0).

along the longitudinal axis z in the form of the parametric solitary wave. Conversely, in the transverse dimensions, the down-converted fields evolve after a transient to a vortex soliton whose transverse stationary profile results from the interplay of diffraction and nonlinearity. Figure 6 illustrates two typical transverse profiles of the signal field in the asymptotic regime of the hybrid solitary wave. As we previously expected (Fig. 2), owing to its nondegenerate configuration, the parametric amplification preserves the vortex structure in the transverse dimension. More precisely, according to the particular phase symmetry of the nondegenerate configuration, the idler vortex has a charge $m=-1$ that is the opposite of that of the signal vortex that was imposed in the initial condition ($m=1$). Note that the vortex background of the signal and idler modes exhibits a rather complicate profile that is related to the envelope reshaping induced by the parametric solitary wave along the longitudinal axis z. Indeed, as shown in Fig. 6(b), the amplitude variation at the edge of the vortex core is no longer monotonic but rather displays a ring shaped hump, a feature termed *halo vortex* in the context of the parametric vortex solitons [7].

We may notice that, as expected, the pump wave does not display a vortex structure in the transverse plane (x,y) in contrast with the signal and idler components [Fig. 7(a)]. In this respect, the vortex solitons considered here are quite different from those considered in Ref. [7]. Here, the prop-
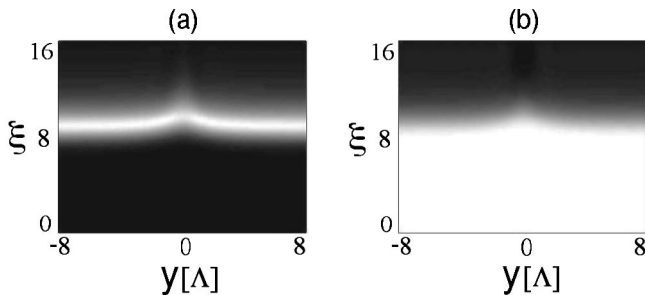

FIG. 4. Same as in Fig. 3, except that the signal (a) and pump (b) amplitudes $|A_{1,3}|$ are plotted in the plane $x=1$ that does not include the vortex core located along the line $(x=0,y=0)$. Parameters are the same as in Fig. 3, the window size is $L=16\Lambda$.
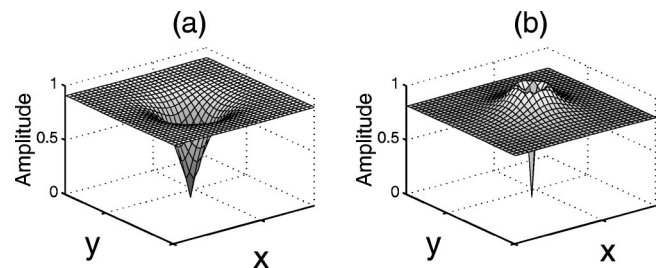

FIG. 6. Typical transverse signal profiles of the 3D hybrid solitary wave at $t=45$: the amplitude $|A_1|$ is plotted in the planes $z=6$ (a) and $z=7$ (b). Parameters are the same as in Fig. 3, the window size is $L=16\Lambda$.
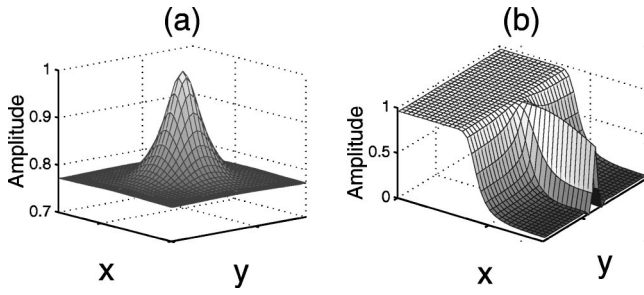
FIG. 7. Typical transverse (a) and longitudinal (b) pump profiles of the 3D hybrid solitary wave at $t=80$: the amplitude $|A_3|$ is plotted in the planes $z=7$ (a) and $x=0$ (b). Parameters are the same as in Fig. 3, the window size is $L=16\Lambda$.

erty of the transverse vortex exhibited by the signal and idler fields is closer to a topological *phase defect* as described in the pioneering work on optical vortex structures in lasers systems [19]. Indeed, in lasers, the nonlinear system is driven far from equilibrium by an external field. Therefore, the analogy between the laser vortices and the 3D hybrid solitary wave reported here can be viewed as follows: The pump wave plays the role of the external field for the signal and idler modes, which see an incoming pump that is continually maintained constant owing to the temporal walkoff between the pump and the down-converted fields. In this view, we may consider the transverse vortex soliton of the down-converted fields to be sustained by the incoming pump in the form of a topological phase defect. This analogy with lasers systems is corroborated by the recent study on topological phase defects in nondegenerate optical parametric oscillators where vector-vortex phase defects, with properties similar to that described here, have been reported [20]. In particular, as in parametric oscillators [21], we may notice in Fig. 7(a) that the transverse distribution of the pump amplitude displays a pulse sitting on a constant background, a feature that may be merely explained by the local frustration of the parametric process due to the zero value of the signal-idler amplitudes imposed by the phase defect.

To complete the description of the 3D hybrid solitary wave, we reported in Fig. 8 the three-dimensional contour plot that illustrates the surface of equal amplitude $|A_{1,3}|$ of the signal and pump fields. Figure 8(a) represents the signal amplitude distribution for $|A_1|=0.8$, it clearly shows that the transverse vortex soliton is localized along the longitudinal z axis. Along this axis, the line of the vortex core where the

signal vanishes appears through a tubular shape in Fig. 8(b), where the isosurface is given at $|A_1|=0.3$. The double-leaf shape that displays the signal in Fig. 8(b) merely reflects the localization of the signal amplitude (i.e., nonmonotonous variation) along the longitudinal z axis. Conversely, the 3D-view of the pump field [Fig. 8(c)] exhibits a single-leaf shape because of the monotonous decreasing of the pump amplitude $|A_3|$ along the z axis (see Fig. 5). Indeed, owing to the parametric process, the plane-wave pump transfers its energy in the whole 3D space except in the proximity of the line of the vortex core where the down-converted fields are compelled to remain small, which prevents the depletion of the pump. This results in the formation of a tubular shape along the line of the vortex core in the 3D view of the pump field [Fig. 8(c)]. Longitudinal and transverse cross sections of the three-dimensional view of the pump field are shown in Figs. 7(a) and 7(b).

Let us finally remark that the hybrid solitary wave does not propagate with the signal group velocity v_1. Indeed, if this was the case, the hybrid solitary wave would not move in the signal reference frame and the numerical simulation would evidence a stationary structure at any time. Conversely, Fig. 3 illustrates a uniform drift of the solitary wave along the axis ξ (i.e., in the signal reference frame), which means that the hybrid solitary wave propagates with a particular selected velocity V_z^*. This is not a surprising result since we have previously shown in the 1D and 2D cases that the parametric solitary wave is subject to a mechanism of velocity selection that results from the interplay of the group-velocity difference between the interacting waves. In the 3D case of interest here, we may easily determine the selected velocity V_z^* in a way akin to the 2D case [15]. Indeed, we may notice that in the regions far from the vortex core, the transverse profile of the hybrid solitary wave displays a flat wavefront where the diffraction effect plays no role. Accordingly, the longitudinal profile of the hybrid solitary wave takes the same shape as in the pure one-dimensional case, as evidenced by the comparison of Figs. 5 and 1. Considering the fact that the 3D hybrid solitary wave propagates without distortion, its velocity V_z^* turns to be the velocity of the pure one-dimensional parametric solitary wave. This velocity may be determined analytically following the Kolmogorov-Petrovskii-Piskunov analysis [22], which has been successfully applied to Brillouin [11] and parametric solitary waves [13,14]. In the particular case of the nondegenerate paramet-
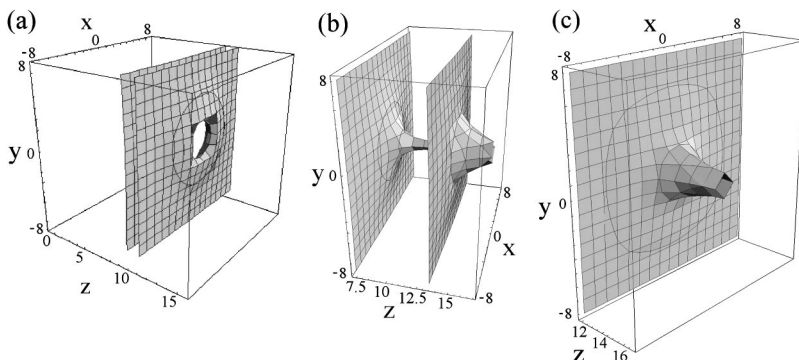

FIG. 8. Three-dimensonal view of the hybrid solitary wave at $t=45$: Surface of equal amplitudes of the signal [(a) $|A_1|=0.8$, (b) $|A_1|=0.3$] and the pump [(c) $|A_3|=0.4$] amplitude distributions. Parameters are the same as in Fig. 3.

ric configuration, this velocity has been determined in Ref. [13], and reads

$$V_z^* = \frac{\mu_2^2 - \mu_1^2 + 4\sqrt{1 - \mu_1 \mu_2}}{4 + (\mu_1 - \mu_2)^2}. \qquad (3)$$

From this expression of the velocity one can easily verify that $-1 < V_z^* < 1$. This means that the velocity v^* of the hybrid solitary wave in the laboratory reference frame and in real physical units, is bounded by the signal velocity v_1 and the pump-idler velocity $v_{2,3}$, i.e., $v_1 < v^* < v_{2,3}$. As for the 2D hybrid solitary wave, the expression (2) of the velocity V_z^* proved to be in excellent agreement with the velocity of the 3D hybrid solitary wave calculated through numerical simulations.

V. STABILITY OF THE VORTEX STRUCTURE

Let us now discuss the important aspect regarding the stability of the transverse vortex structure of the hybrid solitary wave. The stability of the vortex background is closely related to the stability of plane-wave amplitudes that were shown to be always modulationally unstable in quadratic nonlinear media [5–8]. This aspect contrasts with the 3D hybrid solitary wave reported above whose transverse vortex background was revealed to be modulationally stable. Indeed, we have been able to pursue the numerical integration reported in Figs. 3–8 over very long characteristic times of interaction ($t = 200$) and we could not identify any growing modes that would be responsible for the onset of the modulational instability.

1. Influence of the temporal walkoff δ

The mechanism responsible for the stabilization of the vortex background originates in the temporal walkoff between the interacting waves. Owing to the temporal walkoff, the down-converted fields become localized along the longitudinal z axis in the form of the parametric solitary wave (Fig. 5). This suggests that, in the presence of a strong temporal walkoff, the comoving pump and idler amplitudes interact with the localized signal over a very short time, which prevent the onset of modulational instability. Inversely, this reasoning also indicates that, as the temporal walkoff δ decreases, the overlapping of the three fields in the localized structure takes place over a larger time, which would allow for the development of the modulational instability in the vortex background. We may then expect to recover the usual modulational instability of the vortex background for small values of the walkoff parameter δ, in concordance with the previous studies on parametric vortex solitons [5–8].

This prediction may be easily verified by direct numerical simulation of Eqs. (2). Indeed, owing to the normalization adopted in Eqs. (2), the parameters $\kappa_i = v_i \rho_i \sigma_1 e_0 / \delta^2$ simply measure the relative weight of two antagonist effects as regards the stability of the vortex background. On the one hand, the diffraction parameter ρ_i and the pump amplitude e_0 would favor the development of the modulational instability, and on the other hand, the walkoff parameter δ, inversely,
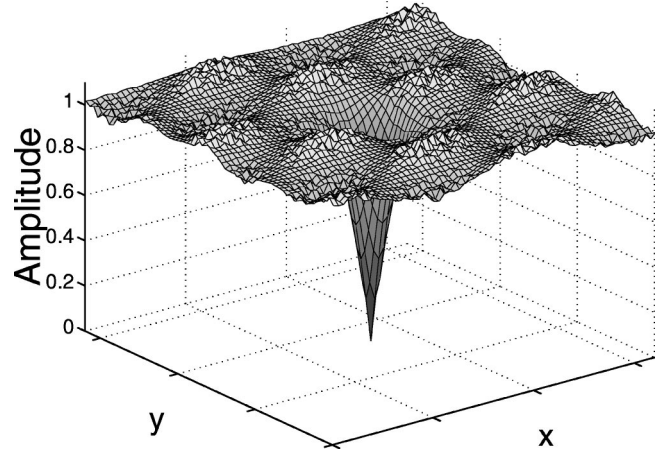

FIG. 9. Instability of the transverse vortex background of the 3D hybrid solitary wave: Transverse signal profile at $t = 35$ for a value of $\kappa = 1.2 \times 10^{-1}$ that is greater than the critical value $\kappa_c \simeq 1.05 \times 10^{-1}$. Other parameters are the same as in Fig. 3.

would quench the modulational instability. We may then expect that, as the parameter κ increases, the 3D hybrid solitary wave reported in Figs. 3–8 would become modulationally unstable. We checked this prediction by solving Eqs. (2) numerically, starting from the same initial condition and for the same parameters as in Figs. 3–8, except that we increased the value of the parameter κ and added a perturbative noise on the initial condition in order to accelerate the development of the modulational instability. A typical result is illustrated in Fig. 9 that represents a transverse vortex profile of the signal amplitude $|A_1|$ for $\kappa = 1.2 \times 10^{-1}$ at time $t = 35$. As expected, the signal field displays the typical modulated pattern in the profile of the vortex background that characterizes the development of the modulational instability. Interestingly, the emergence of the modulational instability proved to be very abrupt with respect to variations of the parameter κ. For the particular values of the damping parameters $\mu_1 = 0.3, \mu_2 = 0.6$ considered in Figs. 3–8, we observed the onset of the modulational instability for values of κ greater than the critical value $\kappa_c \simeq 1.05 \times 10^{-1}$. The existence of a critical value of the parameter κ for the onset of the modulational instability clearly shows the essential role of the temporal walkoff on the stabilization of the vortex soliton embedded in an infinite plane-wave background. Note that, for the sake of simplicity, we restricted our study to the particular case where the pump and idler group velocities are matched ($v_2 = v_3$). However, since the mechanism of stabilization described here originates in the temporal walkoff between the interacting waves, it is also expected to occur in the general case where the three velocities involved in the interaction are different.

It is worth noting that the modulational instability that is discussed here does not occur from plane-wave nonlinear eigenmodes, as in the previous studies of modulational instability in quadratic nonlinear media [5]. The modulational instability of the hybrid solitary wave rather occurs from the specific envelope profile imposed by the parametric solitary wave along the longitudinal z axis. In this respect, the transverse modulational instability encountered here is of the

same nature as that reported in Ref. [23] where the longitudinal profile of the interacting fields is not uniform, but rather displays a periodic pattern associated with the periodic energy conversion and back conversion that characterizes the quadratic nonlinear interaction. Moreover, in the case of the 3D hybrid solitary wave, the fields interact in the presence of the temporal walkoff, which again considerably intricate the study of transverse modulational instability [24].

Also note that the development of the transverse modulational instability has not been observed in the previous study of the 2D hybrid solitary wave because in that work we considered the backward configuration of the parametric process [15]. Owing to the large temporal walkoff δ that is related to the backward interaction, the parameter κ is compelled to remain small, which ensures the stability of the backward 2D hybrid solitary wave. However, due to the technical difficulties encountered in achieving the quasiphase matching in the backward configuration, it would be more convenient to discuss the experimental conditions required for the observation of the hybrid solitary wave in the usual forward configuration of the parametric process. One may generally expect the hybrid solitary wave to be unstable in the forward configuration because of the typical small values of the temporal walkoff δ available in this configuration. However, let us note that there exist particular experimental conditions that may considerably increase the walkoff parameter δ in the forward configuration. As an example, we may consider the configuration of the parametric interaction in which the pump and idler modes are ordinarily polarized while the signal mode is extraordinarily polarized (i.e., type II configuration). In this way, one takes advantage of crystal birefringence in order to increase the temporal walkoff between the signal and the pump-idler waves. Moreover, to avoid the influence of spatial walkoff that has not been included in Eqs. (2), we assume that the crystal operates in the noncritical phase-matching configuration. Under these conditions, we may consider a periodically poled LiNbO$_3$ crystal that is quasiphase matched for the following wavelengths of the three modes $\lambda_1 = 2.35$ μm, $\lambda_2 = 2.9$ μm, $\lambda_3 = 1.3$ μm. For these particular wavelengths, the required period l of the periodically poled LiNbO$_3$ crystal is in the range $l \simeq 27$ μm. Using the dispersion relations (Sellmeier equations) of the LiNbO$_3$ crystal [25] one gets the signal group velocity $v_1 = 1.32 \times 10^8$ m/s, as well as the pump and idler group velocities that turn out to be almost identical $v_2 \simeq v_3 = 1.37 \times 10^8$ m/s. With these velocities, the respective walkoff parameter is $\delta = 2.5 \times 10^6$ m/s and the numerical simulation reported in Figs. 3–8 would correspond to an input pump intensity of $I = 200$ MW/cm^2 (i.e., $e_0 = 32$ MV/m) for an effective nonlinear susceptibility $d = 5$ pm/V. According to this numerical simulation, the 3D hybrid solitary wave is stable and, in view of the realistic experimental data given above, it would be observable in the usual forward configuration of the parametric interaction with currently available technology and nonlinear optical crytals. Note that we considered the particular case of the LiNbO$_3$ crystal to give a specific realistic example, however, we may expect that other nonlinear optical crystals would also be suitable provided that one may exploit their birefringence in order to take advantage of a strong temporal walkoff to ensure the stability of the hybrid solitary wave.

2. Influence of the selected velocity V_z^*

Our numerical simulations reveal that the critical value of the parameter κ_c, above which the hybrid solitary wave becomes unstable, is not a constant value but rather depends on the damping parameters $\mu_{1,2}$ of the down-converted fields. Although this result may be surprising at the first sight, it may be interpreted by the fact that the damping parameters $\mu_{1,2}$ affect the velocity of the hybrid solitary wave V_z^* [Eq. (3)], which in turn affects its stability.

The influence of the selected velocity V_z^* on the stability of the vortex structure may be merely explained as follows: When the hybrid solitary wave propagates with a velocity V_z^* that is closer to that of the signal mode, then the time spent by a given point of the signal amplitude to walk through the localized structure may be large enough to permit the modulational instability to develop. Conversely, when the signal wave rapidly walks away from the localized structure, then the time required for the development of the modulational instability becomes very short, which may prevent the onset of the instability. In other terms, owing to the advection between the modulationally unstable signal field and the localized structure, the modulational instability is drifted out of the localized structure before it has time to develop.

Clearly, the same reasoning also holds when one considers the advection between the hybrid solitary wave and the comoving pump and idler waves. Since the solitary wave velocity v^* is bounded by the signal velocity v_1 and the pump-idler velocity $v_{2,3}$, we may expect that the hybrid solitary wave would be more robust against modulational instability whenever it propagates with the average velocity ($v_1 + v_{2,3})/2$, i.e., with the velocity that minimizes the effective interaction time during which the three fields overlap in the temporally localized structure. We checked this prediction by performing extensive numerical simulations of Eqs. (2). Owing to Eq. (3), we changed the velocity V_z^* by varying the damping parameters $\mu_{1,2}$, and, for each realization we computed the critical value of the parameter κ_c above which the hybrid solitary wave becomes unstable. As expected, we found that the critical value of the parameter κ_c increases as the velocity V_z^* of the hybrid solitary wave approaches zero [i.e., as v^* approaches ($v_1 + v_{2,3})/2$]. According to Eq. (3), we have $V_z^* = 0$ when the damping parameters $\mu_{1,2}$ are chosen such that $\mu_1 + \mu_2 = 2$. For this particular case we found the critical value of the parameter $\kappa_c \simeq 3 \times 10^{-1}$, which is three times the value found in the previous case reported in Figs. 3–8, where the velocity V_z^* of the hybrid solitary wave was closer to the group velocity of the signal wave ($V_z^* = 0.995$). This numerical study confirms the relevant influence of the advection between the hybrid solitary wave and the modulationally unstable field in the mechanism of stabilization of the plane-wave vortex background.

Let us finally mention an analogy between this mechanism of stabilization of a localized structure and a similar mechanism that has been pointed out in the context of stimu-

lated Raman scattering in optical fibers [26]. In that case, the superluminous velocity of the solitary wave is able to walk away from an ''inertial instability'' in a way akin to the 3D hybrid solitary wave, reported here, able to walk away from the modulationally unstable field.

VI. CONCLUSION

In summary, we showed that the three-wave mixing process in quadratic nonlinear media supports 3D hybrid solitary wave solutions in which a transverse vortex soliton is sustained by a longitudinal parametric solitary wave. By invoking simple symmetry considerations, we showed that such a three-dimensional structure can only be sustained by the nondegenerate configuration of the parametric interaction. In contrast to quadratic vortex solitons that were shown to be always modulationally unstable, the 3D hybrid solitary wave proved to be robust with respect to modulational instability. Our numerical analysis reveals that the process of stabilization of the vortex background lies on two mechanisms. On the one hand, the temporal walkoff between the interacting waves leads to a localization of the down-converted fields, which in this way limits the effective interaction time during which the instability may develop. On the other hand, owing to its selected velocity V_z^*, the localized structure is able to walk away from the modulationally unstables fields.

We presented the 3D hybrid solitary wave in the particular context of nonlinear optics because quadratic nonlinear optical crystals constitute ideal test beds for the experimental verification of our predictions. However, the proposed 3D hybrid solitary wave as well as the associated mechanism of self-stabilization are quite general results that may be extended to other physical parametric processes encountered in such diverse fields as hydrodynamics, acoustics, or plasma physics [9]. More recently, it has also been pointed out that the parametric processes play an important role in pattern forming systems subject to a temporal forcing [27] or coupled molecular and atomic Bose-Einstein condensates [28]. In this view, the experimental observation of the 3D solitary wave would be relevant to many branches of nonlinear physics owing to the universality of the resonant wave mixing process.

ACKNOWLEDGMENT

---

[1] L. M. Pismen, *Vortices in Nonlinear Fields* (Clarendon Press, Oxford, 1999).

[2] For a review, see e.g., D. Rozas, C. T. Law, and G. A. Swartzlander, Jr., J. Opt. Soc. Am. B **14**, 3054 (1997), and references therein.

[3] For a review, see e.g., B. Luther-Davies, J. Christou, V. Tikhonenko, and Yu. S. Kivshar;, J. Opt. Soc. Am. B **14**, 3045 (1997); Yu. S. Kivshar and B. Luther-Davies, Phys. Rep. **298**, 81 (1998).

[4] I. V. Basisty, V. Yu.Bazhenov, M. S. Soskin, and M. V. Vasnetsov, Opt. Commun. **103**, 422 (1993); K. Dholakia, N. B. Simpson, M. J. Padgett, and L. Allen, Phys. Rev. A **54**, R3742 (1996); A. Berzanskis, A. Matijosius, A. Piskarskas, V. Smilgevicius, and A. Stabinis, Opt. Commun. **140**, 273 (1997); **150**, 372 (1998); D. V. Petrov and L. Torner, Phys. Rev. E **58**, 7903 (1998); J. Arlt, K. Dholakia, L. Allen, and M. J. Padgett, Phys. Rev. A **59**, 3950 (1999), D. V. Petrov, G. Molina-Terriza, and L. Torner, Opt. Commun. **162**, 357 (1999).

[5] A. V. Buryak and Yu. S. Kivshar, Opt. Lett. **19**, 1612 (1994); Phys. Rev. A **51**, R41 (1995); P. Ferro and S. Trillo, Phys. Rev. E **51**, 4994 (1995); Opt. Lett. **20**, 438 (1995); R. A. Sammut, A. V. Buryak, and Yu. S. Kivshar, J. Opt. Soc. Am. B **15**, 1488 (1998).

[6] T. J. Alexander, A. V. Buryak, and Yu. S. Kivshar, Opt. Lett. **23**, 670 (1998).

[7] T. J. Alexander, Yu. S. Kivshar, A. V. Buryak, and R. A. Sammut, Phys. Rev. E **61**, 2042 (2000).

[8] P. Di Trapani, W. Chinaglia, S. Minardi, A. Piskarskas, and G. Valiulis, Phys. Rev. Lett. **84**, 3843 (2000).

[9] D. J. Kaup, A. Reiman, and A. Bers, Rev. Mod. Phys. **51**, 275 (1979).

[10] J. A. Armstrong, S. S. Jha, and N. S. Shiren, IEEE J. Quantum Electron. **QE-6**, 123 (1970); S. L. McCall and E. L. Hahn, Phys. Rev. Lett. **18**, 908 (1967); K. Drühl, R. G. Wenzel, and J. L. Carlsten, *ibid.* **51**, 1171 (1983); E. Picholle, C. Montes, C. Leycuras, O. Legrand, and J. Botineau, *ibid.* **66**, 1454 (1991).

[11] C. Montes, A. S. Mikhailov, A. Picozzi, and F. Ginovart, Phys. Rev. E **55**, 1086 (1997); C. Montes, A. Picozzi, and D. Bahloul, *ibid.* **55**, 1092 (1997).

[12] A. D. D. Craik, M. Nagata, and I. M. Moroz, Wave Motion **15**, 173 (1992); S. Trillo, Opt. Lett. **21**, 1111 (1996); A. Picozzi and M. Haelterman, *ibid.* **23**, 1808 (1998).

[13] A. Picozzi and M. Haelterman, Europhys. Lett. **45**, 463 (1999).

[14] A. Picozzi and M. Haelterman, Phys. Rev. Lett. **84**, 5760 (2000); Phys. Rev.Lett. **84**, 5760 (2000); **86**, 2010 (2001).

[15] A. Picozzi and M. Haelterman, Phys. Rev. E **59**, 3749 (1999).

[16] Z. H. Musslimani, M. Segev, D. N. Christodoulides, and M. Soljačić, Phys. Rev. Lett. **84**, 1164 (2000); Z.H. Musslimani, M. Segev, and D. N. Christodoulides, Opt. Lett. **25**, 61 (2000); A. H. Carlsson, J. N. Malmberg, D. Anderson, M. Lisak, E. A. Ostrovskaya, T. J. Alexander, and Yu. S. Kivshar, *ibid.* **25**, 660 (2000); J. N. Malmberg, A. H. Carlsson, D. Anderson, M. Lisak, E. A. Ostrovskaya, and Yu. S. Kivshar, *ibid.* **25**, 643 (2000); J. J. Garca-Ripoll, V. M. Prez-Garca, E. A. Ostrovskaya, and Y. S. Kivshar, Phys. Rev. Lett. **85**, 82 (2000); W. Krolikowski, E. A. Ostrovskaya, C. Weilnau, M. Geisser, G. McCarthy, Y. S. Kivshar, C. Denz, and B. Luther-Davies, *ibid.* **85**, 1424 (2000).

[17] X. Liu, L. J. Qian, and F. W. Wise, Phys. Rev. Lett. **82**, 4631 (1999); **85**, 1871 (2000); X. Liu, K. Beckwitt, and F.W. Wise, Phys. Rev. E **62**, 1328 (2000).

[18] C. C. Chow, Physica D **81**, 237 (1995).

[19] P. Coullet, L. Gil, and F. Rocca, Opt. Commun. **73**, 403 (1989).

[20] M. Santagiustina, E. Hernández-García, M. San Miguel, G.-L. Oppo, and A. J. Scroggie (unpublished).

[21] S. Trillo, M. Haelterman, and A. Sheppard, Opt. Lett. **22**, 970 (1997).

[22] V. G. Kolmogorov, I. G. Petrovskii, and N. S. Piskunov, Bull. Univ. Moscow, Ser. Int. Sec. A **1**, 1 (1937); W. van Saarloos, Phys. Rev. Lett. **58**, 2571 (1987).

[23] R. A. Fuerst, D.-M. Baboiu, B. Lawrence, W. E. Torruellas, G. I. Stegeman, S. Trillo, and S. Wabnitz, Phys. Rev. Lett. **78**, 2756 (1997).

[24] P. M. Lushnikov, P. Lodahl, and M. Saffman, Opt. Lett. **23**, 1650 (1998).

[25] V. G. Dmitriev, G. G. Gurzadyan, and D. N. Nikogosyan, *Handbook of Nonlinear Optical Crystals* (Springer-Verlag, Berlin, 1990).

[26] A. Picozzi, C. Montes, and E. Picholle, Phys. Rev. E **58**, 2548 (1998).

[27] D. Walgraef, *Spatio-Temporal Pattern Formation* (Springer, New York, 1997), Chap. 8.

[28] P. D. Drummond, K. V. Kheruntsyan, and H. He, Phys. Rev. Lett. **81**, 3055 (1998); D. J. Heinzen, R. Wynar, P. D. Drummond, and K. V. Kheruntsyan, *ibid.* **84**, 5029 (2000).